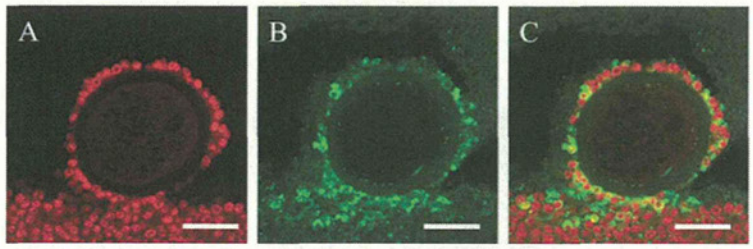

Figure 1 Analysis of natriuretic peptide receptor 2 (NPR2) localisation in porcine ovarian follicles by immunohistochemistry. (*A*) Counterstaining with PI; (*B*) NPR2 staining; (*C*) merged image. Intense positive reaction against anti-NPR2 antibody was observed in oocyte surrounded cumulus cell. Scale bars indicate 100 μm.

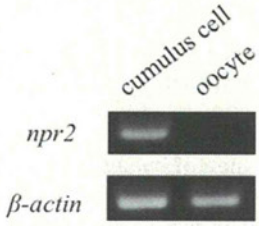

Figure 2 *npr2* mRNA detection in porcine cumulus cells and oocytes. Reverse transcription polymerase chain reaction (RT-PCR) was performed with cDNA prepared from cumulus cells and oocytes. *Npr2* mRNAs were detected only in the cumulus cells but not in the oocytes. The resultant PCR products were separated on a 2% agarose gel and stained with ethidium bromide.

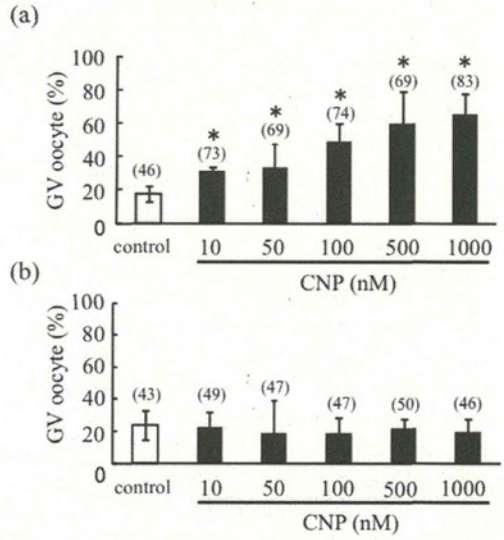

Figure 3 Effect of C-type natriuretic peptide (CNP) on porcine oocyte germinal vesicle breakdown (GVBD) inhibition. Cumulus–oocyte complexes (COCs) (*a*) or denuded oocytes (DOs) (*b*) were further cultured with various concentrations of CNP (10–1,000 nM) for 9 h after 22 h of pre-culture in the presence of dbcAMP. Oocytes were fixed and stained with 1% aceto-orcein, and GVBD occurrence was evaluated. The numbers in parentheses represent the numbers of oocytes examined. Data were analysed by *t*-test. $^*P < 0.05$.

reported changes in *npr2* expression with hormone administration. With oestrogen analogue or equine CG treatment, the *npr2* expression level in granulosa cells was significantly increased. A recent study in mice has shown that CNP stimulates ovarian follicle development (Sato *et al.*, 2012), and a study on *Nppc*- and *Npr2*-mutant mice revealed that lack of the NPPC/NPR2 cascade results in a defective female reproductive system, emphasising the importance of CNP and NPR2 (Kiyosu *et al.*, 2012).

However, while the CNP function has been well established in a rodent model, studies in large domestic animals, including porcine models, have not been done. This result is the first evidence that CNP acts as a meiotic inhibitor in porcine oocytes.

Based on our results showing that *npr2* is expressed in cumulus cells and functions as a CNP receptor, we investigated the regulation mechanism of *npr2* in cumulus cells.

In a previous report in mice, *npr2* expression in cumulus cell was also sustained by the ODPF (Zhang *et al.*, 2010). To demonstrate whether ODPF affects the level of cumulus cell *npr2* expression in the porcine model, we quantitatively compared the level of *npr2* expression in oocytectomised COCs.

As shown in Fig. 4, the relative mRNA expression level of *npr2* was significantly lower than that in the oocytectomised group (OXC) in the COCs group. However, *npr2* mRNA level was restored by co-culture with DOs (OXC + DO), suggesting that porcine ODPF also helps maintain *npr2* expression in cumulus cells. In mice, it has been reported that *npr2* level in cumulus cells was increased by the combination of GDF9, BMP15, and FGF8 (Zhang *et al.*, 2010). In our work, the effects of these factors on *npr2* were not investigated because of the limited availability of these recombinant proteins for porcine studies. Further study is required to identify the main factor(s) involved in the regulation of *npr2* mRNA expression in porcine cumulus cells.

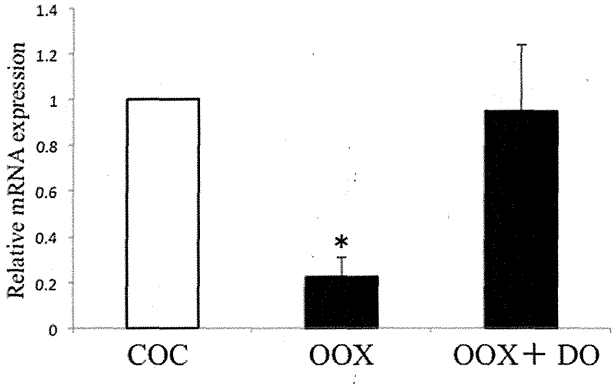

Figure 4 Relative mRNA expression levels of *npr2* in cumulus cells by real-time polymerase chain reaction (PCR) analysis in cumulus–oocyte complexes (COCs), oocytectomised COCs (OXCs), or OXCs with denuded oocytes (DOs) cultured for 24 h. *Npr2* mRNA expression level was normalised to that of β-*actin*. Data are mean ± standard deviation (SD) of three independent experiments. Data were analysed by Bonferroni-Dunn test $^*P < 0.05$.

In summary, our data show that CNP acts as a meiotic inhibitor in porcine oocytes through a mechanism indirectly mediated by cumulus cells. Furthermore, OXCs showed decreased levels of *npr2* mRNA expression, suggesting that ODPF also regulates *npr2* expression in the porcine model. Our finding provides a new insight on the underlying mechanism of meiotic resumption in porcine oocytes and raises the possibility of developing techniques to control *in vitro* maturation in porcine oocytes.

Declaration of interest

None.

Acknowledgement

This work was supported by a grant from the Japan Society for the Promotion of Science to E. Sato (No. 21248032).

References

Ballermann, B.J. & Brenner, B.J (1987). Atrial natriuretic peptide and kidney. *Am. J. Kidney Dis.* **10**, 7–12.

Downs, S.M., Coleman, D.L., Ward-Bailey, P.F. & Eppig, J.J. (1985). Hypoxanthine is the principal inhibitor of murine oocyte maturation in a low molecular weight fraction of porcine follicular fluid. *Proc. Natl. Acad. Sci. USA* **82**, 454–8.

Eppig, J.J. & Downs, S.M. (1987). The effect of hypoxanthine on mouse oocyte growth and development *in vitro*: maintenance of meiotic arrest and gonadotropin-induced oocyte maturation. *Dev. Biol.* **119**, 313–21.

Fan, H.Y., Huo, L.J., Chen, D.Y., Schatten, H. & Sun, Q.Y. (2004). Protein kinase C and mitogen-activated protein kinase cascade in mouse cumulus cells: cross talk and effect on meiotic resumption of oocyte. *Biol. Reprod.* **70**, 1178–87.

Gotze, M., Kauffold, P., Schuffenhauer, A., Torner, H. & Spitschak, M. (1990). [The inhibition of meiosis of bovine oocytes using biologic of synthetic inhibitors.] *Arch. Exp. Veterinarmed.* **44**, 19–27.

Jankowski, M., Reis, A.M., Mukkadam-Daher, S., Dam, T.V., Farookhi, R. & Gutkowska, J. (1997). C-type natriuretic peptide and the guanylyl cyclase receptors in the rat ovary modulated by the estrous cycle. *Biol. Reprod.* **56**, 59–66.

Kadam, A.L. & Koide, S.S. (1990). Identification of hypoxanthine in bovine follicular fluid. *J. Pharm. Sci.* **79**, 1077–82.

Kimura, N., Konno, Y., Miyoshi, K., Matsumoto, H. & Sato, E. (2002). Expression of hyaluronan synthases and CD44 messenger RNAs in porcine cumulus–oocyte complexes during in vitro maturation. *Biol. Reprod.* **66**, 707–17.

Kiyosu, C., Tsuji, T., Yamada, K., Kajita, S. & Kunieda, T. (2012). NPPC/NPR2 signaling is essential for oocyte meiotic arrest and cumulus oophorus formation during follicular development in the mouse ovary. *Reproduction* **144**, 187–93.

Norris, R.P., Ratzan, W.J., Freudzon, M., Mehlmann, L.M., Krall, J., Movsesian, M.A., Wang, H., Ke, H., Nikolaev, V.O. & Jaffe, L.A. (2009). Cyclic GMP from the surrounding somatic cells regulates cyclic AMP and meiosis in the mouse oocyte. *Development* **136**, 1869–78.

Petr, J., Rajmon, R., Chmelíková, E., Tománek, M., Lánská, V., Pribánová, M. & Jílek, F. (2006). Nitric-oxide-dependent activation of pig oocytes: the role of the cGMP-signalling pathway. *Zygote* **14**, 9–16.

Petters, R.M. & Wells, K.D. (1993). Culture of pig embryos. *J. Reprod. Fertil. Suppl.* **48**, 61–73.

Pincus, G. & Enzmann, E.V. (1935). The comparative behavior of mammalian eggs *in vivo* and *in vitro*: I. The activation of ovarian eggs. *J. Exp. Med.* **62**, 665–75.

Potter, L.R., Abbey-Hosch, S. & Dickey, D.M (2006). Natriuretic peptides, their receptors, and cyclic guanosine monophosphate-dependent signaling functions. *Endocr. Rev.* **27**, 47–72.

Rahmutula, D. & Gardner, D.G. (2005). C-type natriuretic peptide down-regulates expression of its cognate receptor in rat aortic smooth muscle cells. *Endocrinology* **146**, 4968–74.

Roh, S.G., Song, S.H., Cho, K.C., Katoh, K., Wittamer, V., Parmentier, M. & Sasaki, S. (2007). Chemerin—a new adipokine that modulates adipogenesis via its own receptor. *Biochem. Biophys. Res. Commun.* **362**, 1013–8.

Sato, Y., Cheng, Y., Kawamura, K., Takae, S. & Hsueh, A.J. (2012). C-type natriuretic peptide stimulates ovarian follicle development. *Mol. Endocrinol.* **26**, 1158–66.

Schmidt, H., Stonkute, A., Jüttner, R., Schäffer, S., Buttgereit, J., Feil, R., Hofmann, F. & Rathjen, F.G. (2007). The receptor guanylyl cyclase Npr2 is essential for sensory

axon bifurcation within the spinal cord. *J. Cell. Biol.* **179**, 331–40.

Schulz, S. (2005). C-type natriuretic peptide and guanylyl cyclase B receptor. *Peptides* **26**, 1024–34.

Törnell, J., Carlsson, B. & Billing, H. (1990). Atrial natriuretic peptide inhibits spontaneous rat oocyte maturation. *Endocrinology* **126**, 1504–8.

Warikoo, P.K. & Bavister, B.D. (1989). Hypoxanthine and cyclic adenosine 5′-monophosphate maintain meiotic arrest of rhesus monkey oocytes *in vitro*. *Fertil. Steril.* **51**, 886–9.

Webb, R.J., Marshall, F., Swann, K. & Carroll, J. (2002). Follicle-stimulating hormone induces a gap junction-dependent dynamic change in [cAMP] and protein kinase A in mammalian oocytes. *Dev. Biol.* **246**, 441–54.

Woodard, G.E. & Rosado, J.A. (2008). Natriuretic peptides in vascular physiology and pathology. *Int. Rev. Cell. Mol. Biol.* **268**, 59–93.

Zhang, M., Su, Y.Q., Sugiura, K., Xia, G. & Eppig, J.J. (2010). Granulosa cell ligand NPPC and its receptor NPR2 maintain meiotic arrest in mouse oocytes. *Science* **330**, 366–9.

Animal Science Journal

Animal Science Journal (2013) **84,** 15–22 doi: 10.1111/j.1740-0929.2012.01030.x

ORIGINAL ARTICLE

Distribution of protein disulfide isomerase during maturation of pig oocytes

Yumi OHASHI, Yumi HOSHINO, Kentaro TANEMURA and Eimei SATO

Graduate School of Agricultural Science, Tohoku University, Aoba, Sendai, Japan

ABSTRACT

Oocyte maturation in mammals is characterized by a dramatic reorganization of the endoplasmic reticulum (ER). In mice, the ER forms accumulations in the germinal vesicle (GV) stage and distinctive cortical clusters in metaphase II (MII) of the oocyte. Multiple evidence suggests that this ER distribution is important in preparing the oocyte for Ca^{2+} oscillations, which trigger oocyte activation at fertilization. In this study, we investigated the time course and illustrated the possible functional role of ER distribution during maturation of porcine oocytes by immunostaining with protein disulfide isomerase (PDI). PDI forms clusters in the cytoplasm of oocytes. After immunostaining, PDI clusters were identified throughout the cytoplasm from the GV to metaphase I (MI) stage; however, at the MII stage, the PDI formed large clusters (1–2 μm) in the animal pole around the first polar body. PDI distribution was prevented by bacitracin, a PDI inhibitor. Our experiments indicated that, during porcine oocyte maturation, PDI undergoes a dramatic reorganization. This characteristic distribution is different from that in the mouse oocyte. Moreover, our study suggested that formation of PDI clusters in the animal pole is a specific characteristic of matured porcine oocytes.

Key words: *endoplasmic reticulum, oocyte maturation, porcine, protein disulfide isomerase.*

INTRODUCTION

A hallmark feature of fertilization in mammalian oocytes is the release of Ca^{2+} from intracellular stores. This phenomenon is termed 'Ca^{2+} oscillation', and is essential for preventing polyspermy, initiating egg activation, and recruiting maternal RNAs that initiate protein synthesis after fertilization (Mann *et al.* 2010). Ca^{2+} oscillations originate in the endoplasmic reticulum (ER); therefore, the ER plays an important role during fertilization.

Oocytes need to complete maturation before fertilization. Oocyte maturation is the final stage of oogenesis, during which the fully mature oocyte develops into a fertilization-competent egg. In mammalian oocytes, this process involves the breakdown of the prophase nucleus (germinal vesicle breakdown; GVBD), formation and migration of the metaphase I (MI) spindle to the oocyte cortex, extrusion of the first polar body, and establishment of the metaphase II (MII) spindle. These nuclear changes are accompanied by various cytoplasmic modifications that render the oocyte capable of development after becoming a fertilized egg (FitzHarris *et al.* 2007). The ER exhibits one of these modifications. It undergoes a dramatic reorganization during oocyte maturation in a diverse array of species from marine worms to starfish, *Xenopus*, rodents, bovine and humans (Mann *et al.* 2010). In the GV stage of the mouse oocyte, the ER is continuous with the nuclear envelope and is present throughout the cytoplasm in small accumulations throughout the oocyte interior. During oocyte maturation to the MII stage, the ER changes such that clusters of 1–2 μm in diameter appear in the cortex opposite the meiotic spindle (FitzHarris *et al.* 2007). In the hamster oocyte, between the GV stage and prometaphase I, the number and size of the surface ER masses increased. After prometaphase I, the surface ER masses gradually dispersed into several much smaller ER clusters near the surface (Shiraishi *et al.* 1995). In humans, GV-stage oocytes contain little cortical ER that is not organized into cortical clusters. In contrast, MII oocytes contained large (2–3 μm in diameter), distinct ER clusters throughout the cortex (Mann *et al.* 2010). In porcines, ER formed a thin layer beneath the plasma membrane, and the layer became more evident and wider in the MII-stage oocytes (Maeda & Yagyu 1997); therefore,

Correspondence: Yumi Ohashi, Laboratory of Animal Reproduction, Graduate School of Agricultural Science, Tohoku University, Aoba, Sendai, Miyagi 981-8555, Japan. (Email: yumiohashi107@gmail.com)
Received 9 December 2011; accepted for publication 21 February 2012.

ER clustering is a common feature observed in mature oocytes, but cluster distribution varies among animal species.

ER distribution in cells can be observed using an ER marker. The distribution or expression level of several markers have been identified; the markers include Hsc70, Hsp40, calnexin and protein disulfide isomerase (PDI) (Tatu & Helenius 1995; Zhang *et al.* 1997; Meunier *et al.* 2002), which is a major ER marker. PDI is an oxidoreductase that was identified first as a highly abundant, essential protein in the lumen of ER, where it catalyzes the formation, reduction and isomerization of disulfide bridges in nascent proteins during their folding process (Gilbert 1998). In the present study, to investigate the role of ER during porcine oocyte maturation, we analyzed the distribution and expression level of ER protein PDI.

MATERIALS AND METHODS

In vitro maturation (IVM) of oocytes

Porcine cumulus-oocyte complexes (COCs) were isolated as described by Kawahara *et al.* (2002). COCs with uniform ooplasm and a compact mass of cumulus cells were selected and placed into modified Dulbecco's phosphate buffered saline (PBS) medium containing 5.56 mmol/L glucose (Wako Pure Chemical Industries, Ltd, Osaka, Japan), 0.33 mmol/L sodium pyruvate (Wako Pure Chemical Industries, Ltd, Osaka, Japan), 0.01 mL/mL antibiotic/antimycotic solution (Sigma-Aldrich, St. Louis, MO, USA), and 4 mg/mL fatty-acid-free bovine serum albumin (BSA; Sigma-Aldrich, St. Louis, MO, USA). This solution was designated as the PB1 medium (Quinn *et al.* 1982). The COCs were washed in the PB1 medium and then cultured in BSA-free North Carolina State University (NCSU)-23 medium for 44 h at 38.5°C in a highly humidified atmosphere of 5% CO_2. For the first 22 h, they were cultured in NCSU-23 medium supplemented with 10 IU/mL pregnant mare serum gonadotropin (PMSG; Serotropin; Aska Pharmaceutical, Ltd, Tokyo, Japan), 10 IU/mL human chorionic gonadotropin (hCG; Puberogen; Daiichi Sankyo, Tokyo, Japan), 0.6 mmol/L cysteine (Sigma-Aldrich, St. Louis, MO, USA), 1.0 mmol/L dibutyryl cyclic adenosine monophosphate (dbcAMP) (Sigma-Aldrich, St. Louis, MO, USA), 5.0 μg/mL insulin (Gibco BRL Life Technologies, Grand Island, NY, USA), 20 mmol β-mercaptoethanol, and 10% porcine follicular fluid. For the subsequent 22 h after the start of culture, COCs were moved to the fresh culture medium, which did not contain dbcAMP and hormone, and cultured for 22 h (total 44 h). During IVM, 25 COCs were cultured with the 250 μL droplets. These culture drops were made in a 35 mm dish (SUMIRON, Osaka, Japan) and were covered with paraffin oil. To inhibit PDI after medium replacement, we added 1.0, 3.0, 5.0, 10 and 20 mmol/L bacitracin (Sigma-Aldrich, St. Louis, MO, USA) to the medium from 22 to 44 h of IVM.

Immunostaining of PDI

GV oocytes were collected immediately after culturing in the second medium, which was considered as 0 h. GVBD, MI and MII oocytes were collected at 6, 12 and 22 h, respectively, after changing to the second IVM medium. The cumulus cells were removed by vortexing the COCs in PB1 medium containing 1 mg/mL hyaluronidase (Sigma-Aldrich, St. Louis, MO, USA). Cumulus-free oocytes were fixed with 4% (w/v) paraformaldehyde for 90 min at 38.5°C. The fixed oocytes were washed three times in PBS and treated overnight with 2% Triton-X100 in PBS at 38.5°C. The oocytes were then briefly washed three times in PBS and treated with the blocking buffer (1% BSA in 0.5% Triton-X100 in PBS) for 60 min at 38.5°C. They were then incubated for 60 min at 38.5°C with rabbit polyclonal antibody to PDI antibody (PDI-ER marker, Abcam, Cambridge, UK) at a dilution of 1:200 in PBS containing 0.1% polyvinyl alcohol (PVA) and 1.0% BSA (PBS-PVA-BSA). After 3 washings with PBS-PVA-BSA, the oocytes were incubated with Alexa Fluor 488-labeled goat anti-rabbit antibody (Molecular Probes, Inc., Eugene, OR, USA) for 60 min at 38.5°C. After repeated washing in PBS, the oocytes were mounted onto a glass slide containing a small volume of PBS-PVA, and stained with 10 μg/mL propidium iodide (PI) in PBS containing 1.0% BSA for a minimum of 60 min to label the chromosomes. Alexa Fluor 488 (488 nm) and PI (615 nm) generate green and red fluorescent signals, respectively. The samples were then viewed using a Bio-Rad MRC-1024 confocal scanning laser microscope mounted on an Axioplan Zeiss microscope. After observing the entire specimen under a microscope, a single photograph was obtained at two or more points. Approximately 100 oocytes were used per treatment. The experiments were repeated a minimum of three times.

Western blot analysis of PDI

For Western blot analysis, PDI, which is a 57-kDa protein, was separated on 8% sodium dodecyl sulfate – polyacrylamide gel electrophoresis (SDS-PAGE) and electroblotted in a semidry blotting apparatus according to the method of Yokoo *et al.* (2002). After electroblotting, the membranes were blocked with 5.0% nonfat milk in Tris-buffered saline Tween-20 (TBS-T) for 60 min at room temperature. After washing with TBS-T, the membranes were incubated with PDI antibody (1:1000) at 4.0°C. The following day, the membranes were washed with TBS-T and reacted with secondary antibody anti-rabbit immunoglobulin G (IgG) (1:20 000; Jackson ImmunoResearch, West Grove, PA, USA) for 60 min at room temperature. The primary and secondary antibodies were diluted in Can Get Signal Immunoreaction Enhancer Solution (Toyobo Co., Ltd, Osaka, Japan). After washing with TBS-T, the chemiluminescence was visualized using an ECL Plus detection system (GE Healthcare (previously Amersham Bioscience), Buckinghamshire, UK). Each treatment was repeated a minimum of three times. Approximately 100 oocytes were used per treatment.

Density of PDI clusters

Density of PDI clusters was measured by the analysis of immunostained images. All images were obtained through confocal microscopy at a point at which the first polar body could be observed. Analyses were performed with ImageJ 1.42 (National Institutes of Health, Bethesda, MD, USA). In order to obtain PDI cluster outlines, we used the 'Threshold' and 'Measure' functions of the software. The densities of the large clusters were calculated as total area of large clusters (1–2 μm)/total area of all PDI clusters.

Statistical analysis

All values were expressed as means with standard errors (SEM) and analyzed using the Tukey-Kramer test following analysis of variance. Differences were considered significant at the 5.0% and 1.0% probability levels. The statistical significance was evaluated using StatView (Abacus Concepts, Inc., Berkeley, CA, USA).

RESULTS

Distribution of PDI during oocyte maturation

To verify the distribution of PDI-labeled ER, we immunostained the ER of oocytes in the GV, GVBD, MI and MII stages. From the GV to the MI stages, PDI was present throughout the cytoplasm (Fig. 1A–C); however, at the anaphase I and telophase I stages, large PDI clusters were present at the animal pole (data not shown), and at the MII stage, the PDI formed distinctively large clusters (approximately 1–2 μm in diameter) in the cytoplasm (Fig. 1D).

Expression of PDI during oocyte maturation

To determine the amount of PDI expression during IVM, we performed Western blot analysis. As shown in Figure 2, PDI was expressed during oocyte maturation. The graph indicates that the amount of PDI expression was not significantly different among the four stages ($P < 0.05$). The graph also indicates that progression of nuclear maturation was associated with an increase in SEM values. The variation of the amount of PDI expression in each stage became larger with the advance of oocyte maturation, and was the largest at MII.

Density of PDI clusters

To verify whether PDI clusters moved with oocyte maturation, we immunostained the ER in oocytes and measured the density of total and large PDI clusters. We observed that large clusters were approximately 1–2 μm in diameter in oocytes (Fig. 3A,B). Moreover, we observed that density of large clusters significantly ($P < 0.05$) increased from immature (GV and MI stages) to matured (MII) stage in oocytes (Fig. 3C).

Determination of the position of PDI clusters

To determine the position of PDI clusters in the oocytes, we next observed MII oocytes using slices from the cortical plain of the animal pole, the equatorial plain, and the cortical plain of the vegetal pole. Distinctive clusters were located in the cytoplasm near the first polar body – the animal pole (Fig. 4A,B). Large clusters were not observed in the vegetal pole (Fig. 4C), but were found in most of the MII-stage oocytes (66.7%, $n = 57$).

Effect of PDI inhibitor on PDI distribution

To verify the importance of PDI activity forming clusters in matured oocytes, we analyzed the effect of different concentrations of the PDI inhibitor, bacitracin, on PDI clusters in MII oocytes. Oocytes exposed to 1 or 3 mmol/L bacitracin (Fig. 5A-b,A-c) formed PDI clusters of similar density to the control (Fig. 5A-a); however, no PDI clusters were observed in oocytes that were exposed to 5 mmol bacitracin (Fig. 5A-d). Moreover, bacitracin significantly inhibited PDI cluster formation in MII oocytes at 5 mmol ($P < 0.05$) (Fig. 5B).

DISCUSSION

In a previous study by Maeda *et al.* changes in the distribution of ER during porcine oocyte maturation have been investigated using fluorescent lipophilic dye (DiI), which labels the continuous ER membrane. They reported that the ER formed a thin layer beneath the plasma membrane. The layer became more evident and wider in the MII-stage oocytes (Maeda & Yagyu 1997). In the present study, we investigated the distribution of PDI, which is an ER marker, during oocyte maturation by immunostaining with PDI antibody, and indicated that PDI formed distinctive large clusters in the cytoplasm. Furthermore, we showed that the change in PDI was not associated with a change of its expression level during oocyte maturation (i.e. only a change in localization takes place).

In the present study, we examined the changes in PDI distribution during porcine oocyte maturation. As shown in Figure 1, the PDI was evenly distributed throughout the cytoplasm from the GV to MI stage of oocyte maturation; however, at the MII stage, the PDI formed distinctively large clusters in the animal pole of the cytoplasm around the first polar body. However, ER protein expression remained at the same level from the GV to MII stage of oocyte maturation (Fig. 2). These results indicate that the distribution of PDI clusters changed during maturation of porcine oocytes which could be related to their cytoplasmic maturation; however, this type of ER distribution seems to be distinct in porcine MII oocytes and different from that in other animal species (Mehlmann *et al.* 1995).

Reports from studies on oocytes of several animal species, from marine worms to starfish, frogs, mice, hamsters and cows, have shown the functional and structural alterations of ER during oocyte maturation (Jaffe & Terasaki 1994; Shiraishi *et al.* 1995; Stricker *et al.* 1998; Terasaki *et al.* 2001; Payne & Schatten 2003; FitzHarris *et al.* 2007; Ajduk *et al.* 2008). In

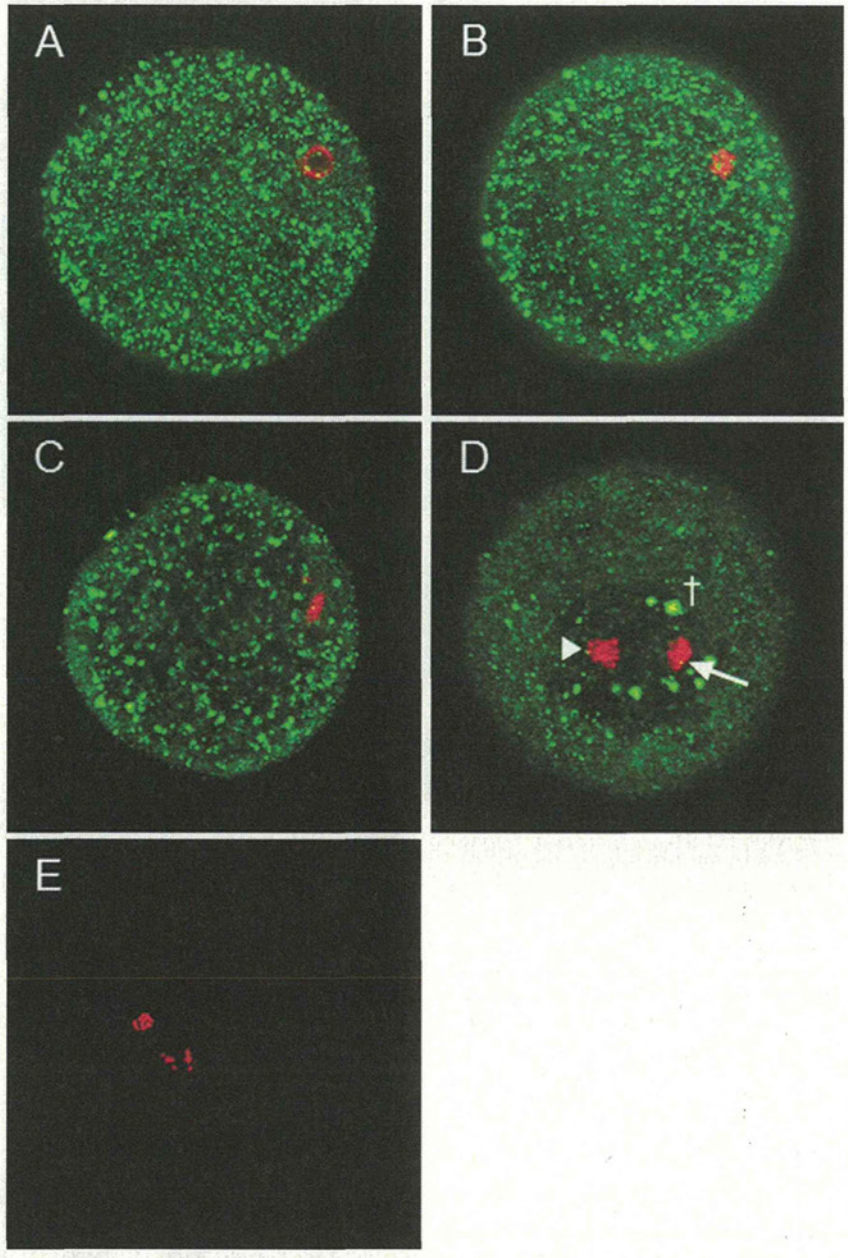

Figure 1 Distribution of protein disulfide isomerase (PDI) during maturation of *in vitro*-matured porcine oocytes. Germinal vesicle (GV) (A) oocyte collected immediately after medium replacement. Germinal vesicle breakdown (GVBD) (B), metaphase I (MI) (C), and metaphase II (MII) (D) collected 6, 12 and 22 h, respectively, after medium replacement. Green and red represent PDI and DNA, respectively. The arrow indicates the first polar body, and the arrowhead indicates the spindle position. The cross indicates the PDI clusters. These images were obtained as whole scans.

GV-stage mouse oocytes, the ER is continuous with the nuclear envelope and is present throughout the cytoplasm, as well as in small accumulations throughout the oocyte interior. During oocyte maturation to the MII stage, the ER changes such that clusters that are 1–2 μm in diameter appear in the cortex opposite the meiotic spindle (vegetal pole) (Mehlmann *et al.* 1995; FitzHarris *et al.* 2007). In the present study, PDI cluster formation was detected in the cortex of the animal pole in porcine MII-stage oocytes (Fig. 4) and this finding was contrary to the distribution of that in mouse oocytes. This fact suggests specific differences in ER distribution in oocytes among mammalian species. The expression of PDI was observed in oocytes without

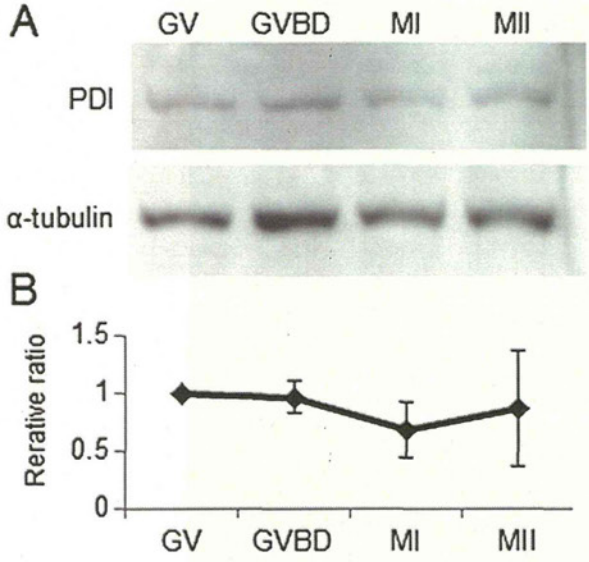

Figure 2 (A) Expression of protein disulfide isomerase (PDI) protein during maturation of porcine oocytes. PDI was detected as a single 57-kDa protein band. α-tubulin was used as an internal control. (B) Time-dependent changes of the level of PDI expression. Values indicate means ± SEM ($P < 0.05$). GV, germinal vesicle; GVBD, germinal vesicle breakdown; MI, metaphase I; MII, metaphase II.

any change in its expression level during maturation (Fig. 2). In a previous study, calreticulin, a major Ca^{2+}-binding chaperone protein, was found to be expressed at relatively higher levels in GV-stage oocytes than in MII-stage oocytes (Zhang *et al.* 2010). This suggests that certain ER proteins show quantitative increases, whereas others show quantitative decreases during nuclear progression.

PDI clusters were distributed around the first polar body at anaphase I and telophase I and after the extrusion of the first polar body, they remained there. These results suggest that PDI cluster has a function for the extrusion of the first polar body.

In a previous study, ER distribution in mouse oocytes changed in parallel to the rearrangement of the ER protein inositol 1,4,5-trisphosphate (IP3) receptor (IP3R) (Mehlmann *et al.* 1995). This protein releases Ca^{2+} from stores in the ER immediately after sperm–egg fusion; therefore, it is believed to play a role in the increased sensitivity to IP3 (FitzHarris *et al.* 2007). In bovine oocytes, IP3R was localized at the subvitelline membrane region as a diffuse and discontinuous pattern in the GV stage; however, from the MI to MII stage, IP3R was observed in the vitelline membrane cortex rather than in the animal pole (Wang *et al.* 2005).

Several studies have reported ER distribution during oocyte maturation using Ca^{2+} channels represented by IP3R (Shiraishi *et al.* 1995; Mehlmann *et al.* 1996;

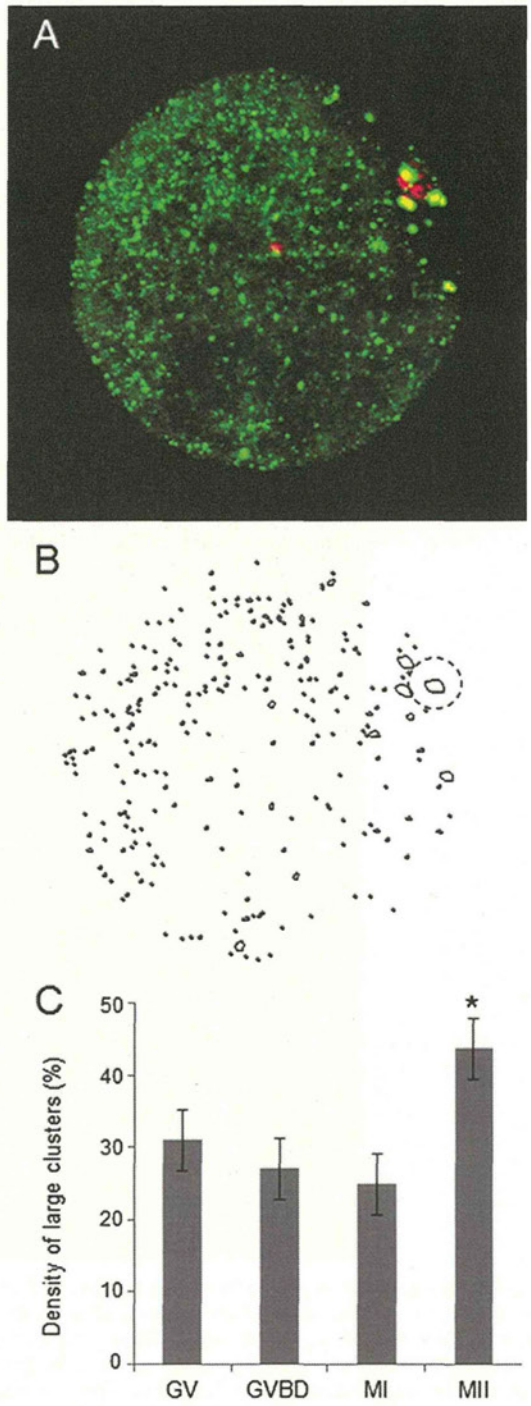

Figure 3 Density of protein disulfide isomerase (PDI) clusters during maturation of porcine oocytes. (A) Porcine metaphase II (MII)-stage oocytes. Green and red represent PDI and DNA, respectively. (B) 'Threshold' image, which makes the cluster outlines clear. The dotted frame indicates large PDI clusters (approximately 1–2 μm in diameter). (C) Density of PDI clusters. The density was calculated as the total area of 1–2 μm PDI clusters/total area of all PDI clusters. Values indicate means ± SEM ($P < 0.05$).

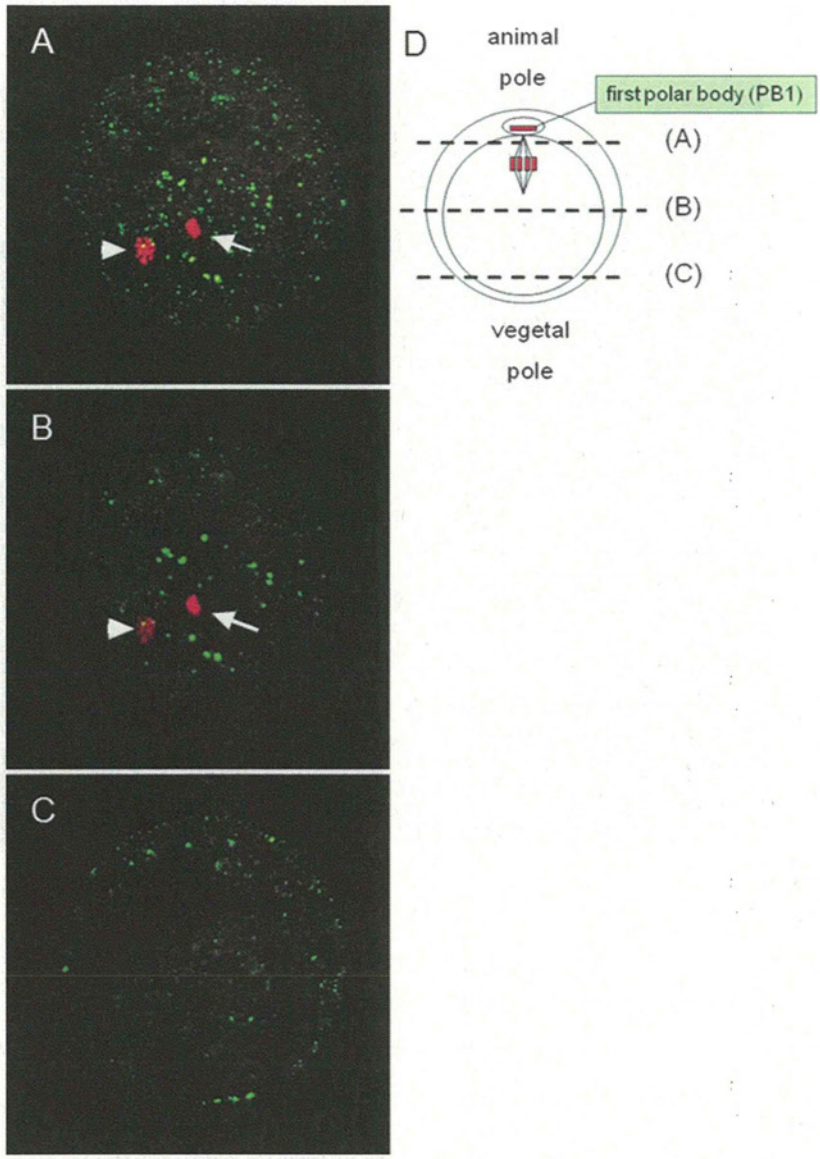

Figure 4 Position of protein disulfide isomerase (PDI) clusters in metaphase II (MII)-stage porcine oocytes matured *in vitro*. MII-stage oocytes were collected 22 h after medium replacement. The animal pole (A), equatorial (B), and the vegetal pole (C) sections are shown as the pattern diagram (D). Green and red represent PDI and DNA, respectively. The arrow indicates the first polar body, and the arrowhead indicates the metaphase plate.

Wang *et al.* 2005). In the present study, we focused on another type of ER protein – PDI. PDI is localized primarily in the ER as a luminal, peripheral membrane protein (Lambert & Freedman 1983) and is known as a major ER marker. It also plays an important role in membrane fusion. PDI has thiol isomerases on its cell surface and catalyzes thiol-disulfide exchange, which activates the fusion of proteins in membranes (Turano *et al.* 2002). Thiol-disulfide exchange is operative in gamete fusion. Gamete fusion requires a sperm surface-associated disulfide isomerase, which could then trigger a protein refolding step along the path to sperm–egg fusion (Ellerman *et al.* 2006).

Bacitracin is a membrane-impermeable PDI inhibitor that has been used over a range of concentrations in somatic cells, and it has been shown to be effective also during gamete fusion (Lahav *et al.* 2003; Markovic *et al.* 2004). When bacitracin-treated oocytes or sperm were preincubated and tested in the *in vitro* fertilization assay, the sperm showed significantly reduced fertilizing ability (Ellerman *et al.* 2006). In the

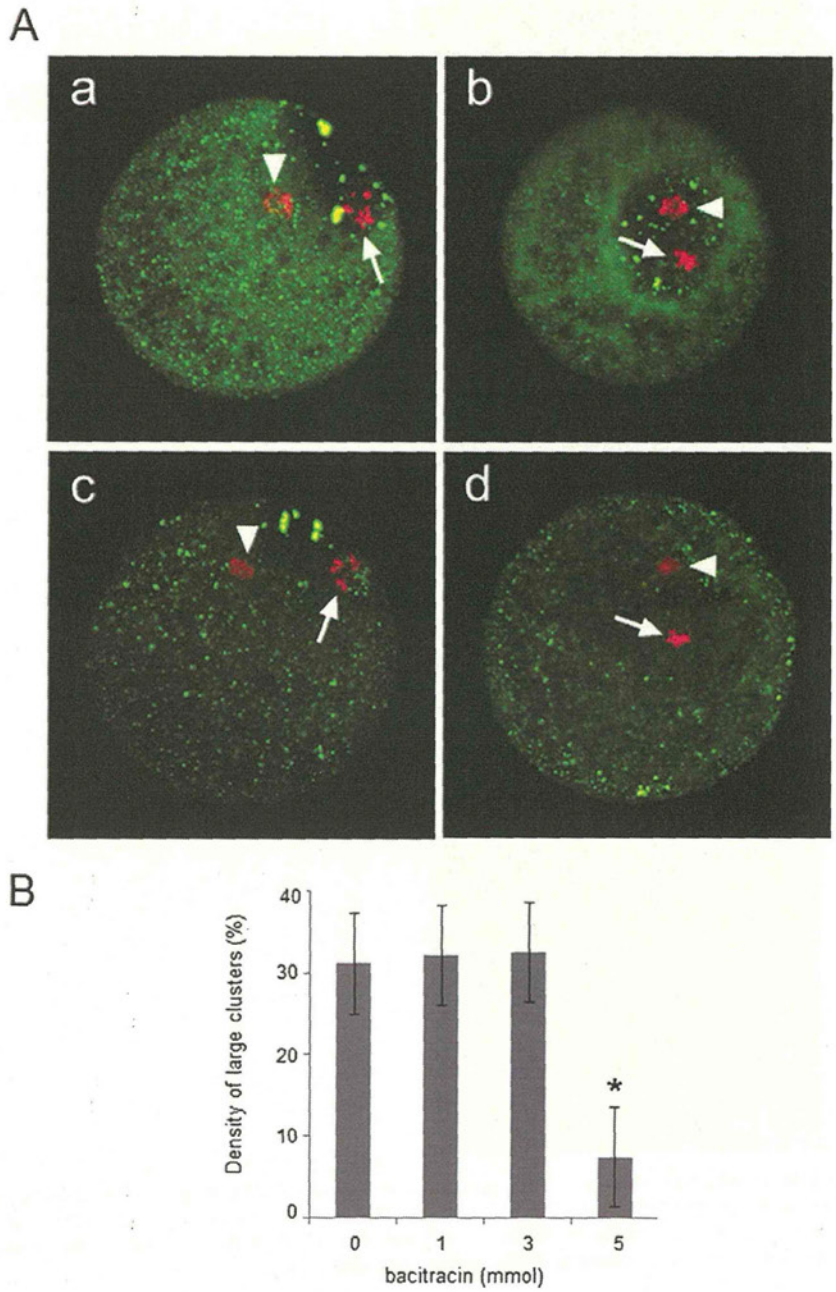

Figure 5 Effect of bacitracin on protein disulfide isomerase (PDI) clusters. After medium replacement, oocytes were cultured in the presence of different concentration of bacitracin for 22 h (A). 0 mm/moL (a), 1.0 mm/moL (b), 3.0 mm/moL (c), 5.0 mm/moL (d). (B) The density of the PDI clusters after culture in the medium containing bacitracin ($P < 0.05$).

present study, we observed that bacitracin inhibited distribution of the PDI clusters (Fig. 5). The result suggests that PDI has a function in the fertilization of the porcine oocyte. Further experiments are needed to clarify the role of PDI in oocytes for maturation, fertilization and embryo development.

Thus, we observed that, in porcine IVM oocytes, ER labeled by PDI staining form large clusters in the animal pole; this feature is specific to MII-stage porcine oocytes.

ACKNOWLEDGMENT

This work was supported by the Japan Society for the Promotion of Science Grant to E. Sato (No. 21248032).

REFERENCES

Ajduk A, Malagocki A, Maleszewski M. 2008. Cytoplasmic maturation of mammalian oocytes: development of a mechanism responsible for sperm-induced Ca^{2+} oscillations. *Reproductive Biology* **8,** 3–22.

Ellerman DA, Myles DG, Primakoff P. 2006. A role for sperm surface protein disulfide isomerase activity in gamete fusion: evidence for the participation of ERp57. *Developmental Cell* **10,** 831–837.

FitzHarris G, Marangos P, Carroll J. 2007. Changes in endoplasmic reticulum structure during mouse oocyte maturation are controlled by the cytoskeleton and cytoplasmic dynein. *Developmental Biology* **305,** 133–144.

Gilbert HF. 1998. Protein disulfide isomerase. *Methods in Enzymology* **290,** 26–50.

Jaffe LA, Terasaki M. 1994. Structural changes in the endoplasmic reticulum of starfish oocytes during meiotic maturation and fertilization. *Developmental Biology* **164,** 579–587.

Kawahara M, Mori T, Tanaka H, Shimizu H. 2002. The suppression of fragmentation by stabilization of actin filament in porcine enucleated oocytes. *Theriogenology* **58,** 1081–1095.

Lahav J, Wijnen EM, Hess O, Hamaia SW, Griffiths D, Makris M, Knight CG, Essex DW, Farndale RW. 2003. Enzymatically catalyzed disulfide exchange is required for platelet adhesion to collagen via integrin $\alpha 2\beta 1$. *Blood* **102,** 2085–2092.

Lambert N, Freedman RB. 1983. Structural properties of homogeneous protein disulphide-isomerase from bovine liver purified by a rapid high-yielding procedure. *Biochemical Journal* **213,** 225–234.

Maeda T, Yagyu T. 1997. Changes in the distribution of endoplasmic reticulum in porcine oocytes during meiotic maturation. *Journal of Mammalian Ova Reserch* **14,** 175–179.

Mann JS, Lowther KM, Mehlmann LM. 2010. Reorganization of the endoplasmic reticulum and development of Ca^{2+} release mechanisms during meiotic maturation of human oocytes. *Biology of Reproduction* **83,** 578–583.

Markovic I, Stantchev TS, Fields KH, Tiffany LJ, Tomic M, Weiss CD, Broder CC, Strebel K, Clouse KA. 2004. Thiol/disulfide exchange is a prerequisite for CXCR4-tropic HIV-1 envelope-mediated T-cell fusion during viral entry. *Blood* **103,** 1586–1594.

Mehlmann LM, Mikoshiba K, Kline D. 1996. Redistribution and increase in cortical inositol 1,4,5-trisphosphate receptors after meiotic maturation of the mouse oocyte. *Developmental Biology* **15,** 489–498.

Mehlmann LM, Terasaki M, Jaffe LA, Kline D. 1995. Reorganization of the endoplasmic reticulum during meiotic maturation of the mouse oocyte. *Developmental Biology* **170,** 607–615.

Meunier L, Usherwood YK, Chung KT, Hendershot LM. 2002. A subset of chaperones and folding enzymes form multiprotein complexes in endoplasmic reticulum to bind nascent proteins. *Molecular Biology of the Cell* **13,** 4456–4469.

Payne C, Schatten G. 2003. Golgi dynamics during meiosis are distinct from mitosis and are coupled to endoplasmic reticulum dynamics until fertilization. *Developmental Biology* **264,** 50–63.

Quinn P, Barros C, Whittingham DG. 1982. Preservation of hamster oocytes to assay the fertilizing capacity of human spermatozoa. *Journal of Reproduction and Fertility* **66,** 161–168.

Shiraishi K, Okada A, Shirakawa H, Nakanishi S, Mikoshiba K, Miyazaki S. 1995. Developmental changes in the distribution of the endoplasmic reticulum and inositol 1,4,5-trisphosphate receptors and the spatial pattern of Ca^{2+} release during maturation of hamster oocytes. *Developmental Biology* **170,** 594–606.

Stricker SA, Silva R, Smythe T. 1998. Calcium and endoplasmic reticulum dynamics during oocyte maturation and fertilization in the marine worm *Cerebratulus lacteus*. *Developmental Biology* **203,** 305–322.

Tatu U, Helenius A. 1995. Interactions between newly synthesized glycoproteins, calnexin and a network of resident chaperones in the endoplasmic reticulum. *Journal of Cell Biology* **136,** 555–565.

Terasaki M, Runft LL, Hand AR. 2001. Changes in organization of the endoplasmic reticulum during Xenopus oocyte maturation and activation. *Molecular Biology of the Cell* **12,** 1103–1116.

Turano C, Coppari S, Altieri F, Ferraro A. 2002. Proteins of the PDI family: unpredicted non-ER locations and functions. *Journal of Cell Physiology* **193,** 154–163.

Wang L, White KL, Reed WA, Campbell KD. 2005. Dynamic changes to the inositol 1,4,5-trisphosphate and ryanodine receptors during maturation of bovine oocytes. *Cloning and Stem Cells* **7,** 306–320.

Yokoo M, Miyahayashi Y, Naganuma T, Kimura N, Sasada H, Sato E. 2002. Identification of hyaluronic acid-binding proteins and their expressions in porcine cumulus-oocyte complexes during *in vitro* maturation. *Biology of Reproduction* **67,** 1165–1171.

Zhang DX, Li XP, Sun SC, Shen XH, Cui XS, Kim NH. 2010. Involvement of ER-calreticulin-Ca^{2+} signaling in the regulation of porcine oocyte meiotic maturation and maternal gene expression. *Molecular Reproduction and Development* **77,** 462–471.

Zhang JX, Braakman I, Matlack KE, Helenius A. 1997. Quality control in the secretory pathway: the role of calreticulin, calnexin and BiP in the retention of glycoproteins with C-terminal truncations. *Molecular Biology of the Cell* **8,** 1943–1954.

Theriogenology 79 (2013) 116–126

Contents lists available at SciVerse ScienceDirect

Theriogenology

journal homepage: www.theriojournal.com

Restoration of corpus luteum angiogenesis in immature hypothyroid *rdw* rats after thyroxine treatment: Morphologic and molecular evidence

Guido Macchiarelli [a,*], Maria Grazia Palmerini [a], Stefania Annarita Nottola [b], Sandra Cecconi [a], Kentaro Tanemura [c], Eimei Sato [c]

[a] *Department of Life, Health and Environmental Sciences, University of L'Aquila, L'Aquila, Italy*
[b] *Department of Anatomy, Histology, Forensic Medicine and Orthopaedics, Laboratory of Electron Microscopy "Pietro M. Motta", University La Sapienza, Rome, Italy*
[c] *Laboratory of Animal Reproduction, Graduate School of Agricultural Science, Tohoku University, Sendai 981-8555, Japan*

ARTICLE INFO

Article history:
Received 2 April 2012
Received in revised form 16 September 2012
Accepted 17 September 2012

Keywords:
Thyroxine
Angiogenesis
Corpus luteum
Pericyte
Electron microscopy
RT-PCR

ABSTRACT

Thyroxine (T4) plus gonadotropins might stimulate ovarian follicular angiogenesis in immature infertile hypothyroid *rdw* rats by upregulating mRNA expression of major angiogenic factors. Development of growing corpus luteum (CL) is strongly related to angiogenesis and to morphofunctional development of microcirculation. Our aim was to investigate if T4 is involved in CL angiogenesis and in the activation of capillary cells and angiogenic factors after ovulation in a spontaneous model of hypothyroidism, the *rdw* rat. *Rdw* rats were treated with T4 plus gonadotropins (equine chorionic gonadotropin plus human chorionic gonadotropin; eCG+hCG) or gonadotropins alone in order to evaluate the effects of T4 on early luteal angiogenesis, on microvascular cells and on expression of major growth factors which are involved in the regulation of angiogenesis. Wistar-Imamichi rats treated with gonadotropins were used as controls. The ovaries were collected 4 days after hCG administration and analyzed using morphologic and molecular approaches. Thyroxine plus gonadotropins stimulated the growth of CLs and follicles as in controls, differently from *rdw* rats treated only with gonadotropins, in which CLs were not found and only small follicles, often atretic, could be recognized. In T4 plus gonadotropin-treated *rdw* rats CLs showed increased microvasculature, numerous activated capillaries characterized by sprouting and other angiogenic figures, and associated pericytes. Quantitative analysis revealed that the number of pericytes in T4 plus gonadotropin-treated *rdw* rats was comparable with that found in control rats and was significantly higher than that found in gonadotropin-treated *rdw* rats. The mRNA expression of vascular endothelial growth factor and basic fibroblast growth factor was significantly higher in control rats and in T4 plus gonadotropin-treated *rdw* rats than in gonadotropin-treated *rdw* rats. mRNA expression of tumor necrosis factor α, transforming growth factor β, and epidermal growth factor did not show significant changes. Our data originally demonstrated that T4 promoted the growth of an active microcirculation in developing CLs of gonadotropin-primed hypothyroid *rdw* rats, mainly by inducing sprouting angiogenesis, pericyte recruitment, and upregulation of mRNA expression of vascular endothelial growth factor and basic fibroblast growth factor. In conclusion, we suggest that T4 plays a key role in restoring luteal angiogenesis in ovaries of immature hypothyroid *rdw* rats.

1. Introduction

Folliculogenesis, ovulation, and corpus luteum (CL) formation are cyclically related to phenomena of microvascular growth, remodeling and regression of blood vessels, and therefore to specific functional changes of the ovarian microcirculation. All these adaptations are fundamental to ensure fertility and normal ovarian function [1–5].

Angiogenic remodeling is particularly intense after ovulation, when new vessels develop from the pre-existing

* Corresponding author. Tel.: +39 0862433652; fax: +39 0862433785.
E-mail address: gmacchiarelli@cc.univaq.it (G. Macchiarelli).

0093-691X/$ – see front matter © 2013 Elsevier Inc. All rights reserved.
http://dx.doi.org/10.1016/j.theriogenology.2012.09.016

thecal vasculature to sustain the development of the initial CL [6–12]. CL is a highly vascularized structure that receives the greatest blood flow per unit of tissue of any organ in the body [12]. As a consequence, the rate of tissue growth and cell proliferation in growing CLs is equal to or even greater than that of the most rapidly growing and dangerous tumors [13]. Pericytes represent a large proportion of proliferating cells in growing CLs [14] and they act as guiding structures aiding the outgrowth of endothelial cells during luteal development [15]. The CL development and functionality is also ensured by the release into luteal cells of intercellular vesicles—secreted by vascular pericytes—containing a high quantity of Thy-1^+ differentiation protein, a morphoregulatory molecule associated with cell differentiation [16].

The angiogenic process is finely regulated by several hormones and growth factors that act as either stimulatory or inhibitory factors [2,3]. In the mammalian ovary, the main regulators of angiogenesis are represented by gonadotropins (follicle [FL] stimulating hormone [FSH] and luteinizing hormone [LH]) and several angiogenic factors including vascular endothelial growth factor (VEGF) [17,18]. The ovary locally produces several other growth factors with angiogenic properties such as: transforming growth factor β (TGFβ) epidermal growth factor (EGF) and tumor necrosis factor (TNF)-α [17]. Recent findings demonstrated that the thyroid hormone, thyroxine (T4), also plays a key role in ovarian FL angiogenesis [19]. It is well known that hypothyroidism is associated with infertility problems, ranging from anovulatory cycles, and sterility to abortion in many mammals and humans [20–22]. Such anomalies could be partially or totally restored by T4 administration [23] or by a combined therapy with T4 including gonadotropins, as reported in hypothyroid women [21] and in a well established model of congenital hypothyroidism, the *rdw* rat [19,24,25].

Numerous studies highlighted that T4 is actively involved in coronary and brain angiogenesis [26–28]. The mechanism of thyroid hormone-induced angiogenesis is initiated with integrin αVβ3 receptor [29] after T4 binding and involves the secretion of basic fibroblast growth factor (bFGF) and VEGF by endothelial cells, as recently reviewed [30]. In the ovary of immature female *rdw* rats, T4 markedly improved the development of follicular microvasculature, especially in the presence of eCG, by regulating the gene expression of some growth factors involved in the regulation of angiogenesis, such as VEGF, TNFα, bFGF, and of their receptors [19]. However, although it was demonstrated that T4 therapy supports the formation of functional CL and the establishment of normal pregnancy in hypothyroid rodents [31], the effect of this hormone on ovarian luteal angiogenesis has not yet been addressed.

In this study we tested the hypothesis that T4 might mediate the development of CL microcirculation in immature infertile hypothyroid *rdw* rat ovaries and mRNA expression levels of main ovarian angiogenic growth factors such as VEGF, TGFβ-1, bFGF, EGF, and TNFα.

To this aim, we performed: (1) a structural and ultrastructural study by light microscopy (LM), transmission electron microscopy (TEM), and scanning electron microscopy (SEM) of vascular corrosion casts (vcc) to analyze the ovarian microvasculature, evaluated especially in terms of capillary activation and pericyte recruitment [1,4,19]; (2) a quantitative analysis to determine the number of pericytes in follicular and luteal capillaries [5]; (3) a semiquantitative reverse-transcriptase polymerase chain reaction (RT-PCR) to analyze the mRNA expression of VEGF, TGFβ-1, bFGF, EGF, and TNFα, all involved in gonadotropin-stimulated luteal angiogenesis [2,3,13,19,32].

2. Materials and methods

2.1. Animals

Infertile immature hypothyroid *rdw* rats (N = 12; six per each experimental group), and their normal littermates (Wistar-Imamichi rats; [control] N = 4) were used. Animals were produced and maintained as previously described [19,24,25,31]. The *rdw* mutants were distinguished according to low body weight, retarded development of ears, and small body size at approximately 2 weeks of age. This study conformed to the Ethics Committee for Care and Use of Laboratory Animals for Biomedical Research of the Faculty of Agricultural Sciences, Tohoku University, Japan and to the E.C. regulation on this matter.

2.2. Experimental groups and hormonal treatments

Group 1 included Wistar-Imamichi rats, treated with eCG and hCG to induce superovulation and CL formation, used as control rats. Female immature *rdw* rats were divided randomly and treated as follows [24]: group 2, eCG and hCG; group 3, T4 and eCG and hCG.

eCG (10 IU) (Sankyo Kabu Company, Tokyo) was injected subcutaneously on Day 28 after birth; hCG (10 IU) (Sankyo Kabu Company, Tokyo) was given intraperitoneally (ip) 54 hours after eCG administration. Thyroxine (L-thyroxine, Sigma Chemical Company, St. Louis, MO, USA) was administered intraperitoneally (ip) once a day at a dose of 10 mg per 100 g of body weight, from Day 21 to Day 30 [19]. Thyroxine was dissolved in 2 mol NaOH and prepared in physiological saline solution (pH 8.3). The animals were sacrificed 4 days after hCG administration to study CL angiogenesis in the period of maximal expression (i.e., in the developing CL).

2.3. Experimental design

2.3.1. Morphologic study

2.3.1.1. Light microscopy and TEM. To assess the cellular morphologic changes of CL formation and ovarian microvasculature, LM (in semithin sections) and TEM (in ultrathin sections) studies were conducted as described previously [4,5,19]. Budding and sprouting (activated) capillaries were considered proliferative (angiogenic), and regular capillaries were considered quiescent. Proliferating and quiescent capillaries were classified on the basis of the whole capillary vessel ultrastructure, giving a special attention to the endothelial cell morphology (shape, plasma membrane specialization, nucleus morphology, and cytoplasmic

organelle amount). Capillary lumen restriction (pocket-like lumen), as well as the occurrence of capillary buds and sprouts were considered a morphologic feature of sprouting angiogenesis [4,5].

2.3.1.2. Scanning electron microscopy of vcc. CL microvascular architecture and the distribution of angiogenic and angioregressive figures were evaluated by SEM of vcc. Vessels were classified according to their diameter and shape [4,6–9]. Budding, sprouting, and splitting of capillaries from pre-existing blood vessels were considered proliferative (angiogenic) figures [5–8,33]. Incompletely filled or thin capillaries were considered degenerative figures [4,7,34].

2.3.2. Quantitative study of pericytes

Approximately sixty cross-sectioned capillaries, formed by three or fewer endothelial cells and not surrounded by vascular smooth muscle, were selected from semithin sections obtained from at least five different CLs and/or FLs of two control and eight *rdw* rats [35]. Capillaries of FLs were counted in morphologically healthy theca layers of antral to mature FLs. Interstitial (stromal) capillaries were excluded from the evaluation. Pericytes were distinguished from other cell types and enumerated according to morphologic features (shape, presence of cellular processes) and spatial distribution around the outer endothelial cell membrane. The number of capillaries and pericytes from FLs and CLs was summed to obtain the total number in the so called "follicular-luteal complex" [36], because it is from the invasion of thecal capillaries into the avascular antral cavity from which the subsequent luteal structure is originated. The Image J software (National Institutes of Health, Bethesda, MD, USA) was used to estimate the medium number of pericytes (mural cells) in each counted capillary.

2.3.3. Molecular study

mRNA expression levels of the following growth factors which are involved in the regulation of angiogenesis: VEGF, TGFβ-1, bFGF, EGF, and TNFα, were determined in *rdw* rats by RT-PCR and compared with those of control rats as previously reported [19].

2.4. Animal preparation and sample processing

Perfusion of rats (N = 8 *rdw* and N = 2 control rats) was carried out as previously described [6–8]. Briefly, animals were anesthetized with 50 mg/kg body weight ip pentobarbital sodium (50 mg/mL). The aorta was cannulated and a physiological saline solution containing heparin and 1% glutaraldehyde was allowed to flow into it. At the same time, the inferior vena cava was cut to allow the drainage of blood.

2.5. Light microscopy and TEM methods

After perfusion, one ovary per each animal was promptly fixed in 2.5% glutaraldehyde, postfixed with 1% osmium tetroxide, dehydrated in a graded ethanol series, and embedded in Agar resin as previously reported [19,36]. Sections were cut with Ultracut E-Reichert-Jung ultramicrotome. For LM, 1 μm-thick sections of the embedded tissues were stained with aqueous methylene blue, examined, and photographed with a Zeiss Ultraphot II microscope. For TEM observations, ultrathin sections of 0.11 to 0.13 μm in thickness were prepared on unsupported copper grids and stained with uranyl acetate and lead citrate. Specimens were observed and photographed with a Zeiss EM 10A microscope.

2.6. Scanning electron microscopy of vcc method

After perfusion, Mercox resin (Okenshoji Co. Ltd., Tokyo, Japan) was slowly injected into the aorta until polymerization started [19,37]. The casted ovaries (N = 1 per each animal) were removed and placed in a warm water bath to complete polymerization, corroded in a 10% NaOH solution at 60 °C for 24 to 48 hours, and gently washed for 2 to 3 hours under tap water. Then, samples were immersed in distilled water for 2 to 3 days at 60 °C to completely remove macerated tissues, and washed again under running tap water. Half of the samples were frozen at −18 °C and cut with a cooled razor blade, to allow the visualization of the internal structures of the casts. All samples were air dried, mounted on aluminum stubs and coated with platinum in an Emitech cold sputter coater at 20 mA for 2.5 minutes [6–8]. The observations were performed at low accelerating voltage (3–7 kV), in FE Hitachi S-4000 and S-4200 Field Emission Scanning Electron Microscopes.

2.7. Semiquantitative RT-PCR assay

Four days after hCG administration (postnatal day 34), the ovaries were collected from two animals from each experimental group and rapidly frozen in liquid nitrogen and then stored at −80 °C until assay. The semiquantitative

Table 1
Quantitative study of pericytes.

	Group 1		Group 2		Group 3	
	FLs	CLs	FLs	CLs	FLs	CLs
FLs/CLs evaluated	3	3	5	-	3	3
Capillaries	20 ± 3	19.3 ± 3.2	19.2 ± 1.9	-	19.7 ± 2.1	20 ± 3.6
Total capillaries	19.7 ± 2.8		19.2 ± 1.9		19.8 ± 2.6	
Pericytes	12.7 ± 1.5[a]	14 ± 1[b]	8.2 ± 1.3[c]	-	13 ± 2.6[a]	14.7 ± 1.2[b]
Total pericytes	13.3 ± 1.4[a]		8.2 ± 1.3[c]		13.8 ± 2[a]	

Data are shown as N and mean ± SD. Approximately 60 cross-sectioned capillaries, formed by three or fewer endothelial cells, were selected from semithin sections obtained from at least five different corpora lutea (CLs) and/or follicles (FLs) of two control and eight *rdw* rats. Different superscript letters indicate significant differences among experimental groups ($P < 0.001$).

RT-PCR assay was done as previously described on whole frozen ovaries [19]. Briefly, total cellular RNA was extracted from each frozen specimen with RNeasy Mini Kit (Qiagen K.K., Tokyo, Japan), treated with DNase I on RNeasy Mini Spin Columns to avoid DNA contamination. RNA was quantified using an ultraviolet-visible recording spectrophotometer (UV-160, Shimadzu Corporation, Tokyo, Japan). Semiquantitative RT-PCR was performed using Ready To Go RT-PCR Beads (Amersham Pharmacia Biotech, Inc., Piscataway, NJ, USA). One microgram of total RNA per sample was reverse transcribed by one-step protocol according to manufacturer's instructions. The RT reaction was carried out at 42 °C for 15 minutes, and samples were incubated for reaction at 95 °C for 5 minutes to inactivate the reverse transcriptase and to completely denature the template. Primer pairs for VEGF, TGFβ-1, bFGF, EGF, TNFα, and for 18S (488 base pairs) were used (Ambion Inc., Austin, TX, USA) [19]. The amplification cycle consisted of 95 °C for 1 minute, 60 °C for 1 minute, and 72 °C for 2 minutes. After 30 cycles of amplification, each PCR product was electrophoresed in a 2% agarose gel for approximately 35 minutes. The gels were stained in 1% EtBr for 45 min and pictures were taken. The bands were quantified by densitometry using NIH Image 1.63 analysis program (National Institutes of Health). Each gene mRNA level was normalized against its respective 18S mRNA and expressed as fold difference.

2.8. Statistical analysis

Quantitative data in Table 1 and semiquantitative RT-PCR data were analyzed by one way ANOVA followed by Tukey's multiple comparison test as a post test (GraphPad Prism 6). Differences with $P < 0.05$ were considered statistically significant.

3. Results

3.1. Morphological study

3.1.1. Group 1: Gonadotropin-treated Wistar-Imamichi rats (control)

By LM, control rats presented numerous FLs at different stages of growth and a few CLs (Fig. 1A). Developing CLs presented clusters of luteal cells characterized by cytoplasmic lipid droplets and interspersed in a richly vascularized connective tissue (Fig. 1A). Numerous follicular and luteal capillaries, as well as venules and arterioles of various caliber were found. The capillaries were mainly rounded, composed of 2 to 3 endothelial cells, surrounded by some pericytes (Fig. 1A, inset).

By TEM, endothelial cells of luteal capillaries showed an irregular luminal surface with numerous luminal thin and short projections, a cytoplasm with a few organelles and irregularly shaped nuclei. The capillary pericytes were provided with thin and long extensions that surrounded the endothelial cells and by round or ovoid nuclei (Fig. 2A). Endothelial cells of arterioles and venules were polyhedral, with irregularly shaped nuclei, and numerous luminal and abluminal thin, short cytoplasmic processes (Fig. 3A, B). By SEM of vcc four to six vascular plexuses (VPs) were identified on the ovarian surface of control rats. CLs showed

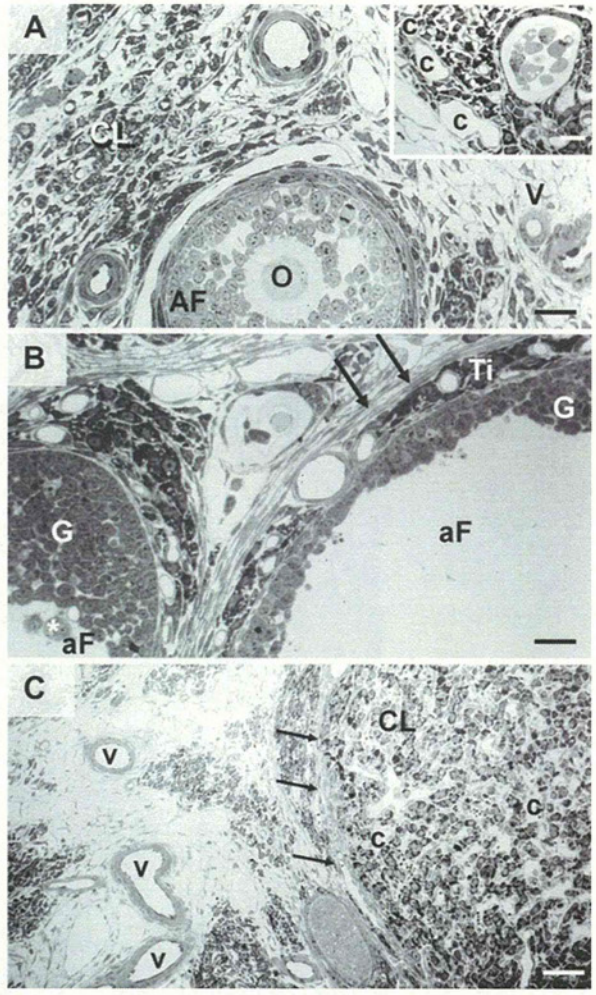

Fig. 1. Representative images of the rat ovarian cortex by light microscopy. (A) Group 1: gonadotropin-treated Wistar-Imamichi rats (control). A healthy antral follicle (AF) with the enclosed oocytes (O) is shown. The cortex is supplied by numerous stromal vessels (v) interspersed in the connective tissue. A richly vascularized developing CL, partially sectioned, is also visible. Bar, 50 μm. (Inset) A higher magnification of a developing CL. The luteal tissue is composed of clusters of luteal cells with a granular cytoplasm rich in lipid droplets, and it is highly vascularized. c, capillaries. Bar, 50 μm. (B) Group 2: gonadotropin-treated *rdw* rats. Atretic antral follicles (aF) with fluctuant granulosa cells into the follicular antrum (asterisk). An irregular circular profile characterizes these follicles. Note that the degenerative processes involve both granulosa cells (G) (follicle wall irregular in shape and thickness) and the theca layers, that appear thin and disorganized. TI, theca *interna*. Arrows indicate theca *externa*. Bar, 100 μm. (C) Group 3: Thyroxine plus gonadotropin-treated *rdw* rats. A richly vascularized corpus luteum (CL), as evidenced by numerous capillaries (c). Stromal veins (v) drained the blood flow outside the capsule of connective tissue (arrows) surrounding the CL. Bar, 100 μm.

a dense vascular network made of small caliber capillaries growing toward the antral cavity (Fig. 4A).

3.1.2. Group 2: Gonadotropin-treated rdw rats

By LM, numerous atretic antral FLs and some healthy antral FLs were seen (Fig. 1B). CLs were not found. Atretic antral FLs appeared irregularly shaped and encircled by irregular theca layers (Fig. 1B). Different to group 1, the boundary line between theca *interna* and theca *externa*

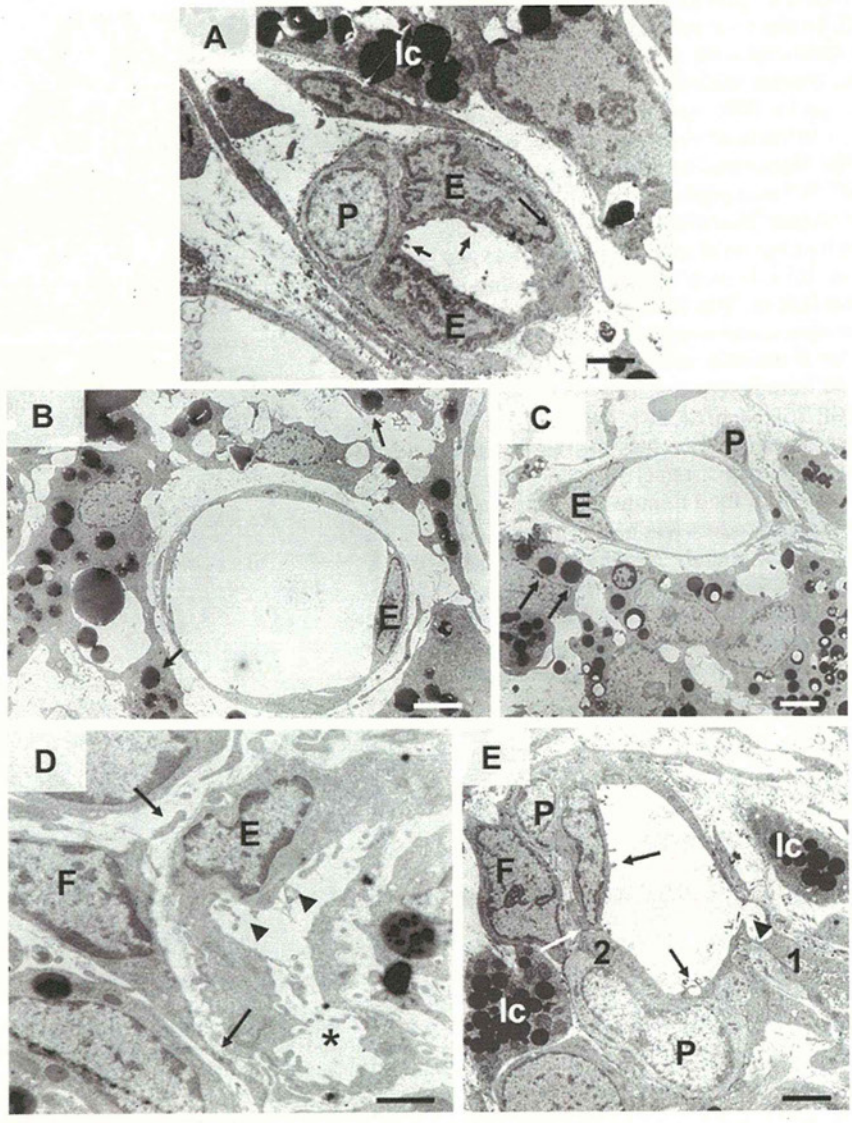

Fig. 2. Representative images of rat ovarian capillaries by transmission electron microscopy. (A) Group 1: gonadotropin-treated Wistar-Imamichi rats (control). A luteal capillary showing signs of angiogenic activation is shown. Endothelial cells (E) present irregular cytoplasmic protrusions (arrows) in the luminal surface of the plasma membrane. A pericyte (P) envelops endothelial cells with its protrusions within the microvascular basement membrane of the capillary. Luteal cells (lc) are also visible in the section. Bar, 5 μm. (B) and (C) Group 2: gonadotropin-treated *rdw* rats. Quiescent capillaries in the theca *interna* of atretic follicles. (B) The capillary shows a roundish and regular profile in section. Endothelial cells (E) are thin and flat. Bar, 5 μm. (C) a small pericyte (P) is in close proximity to the capillary and partially envelops the endothelial cell (E) with its cytoplasmic protrusions. Arrows: thecal cells showing signs of luteinization, as indicated by the accumulation of electron-dense lipid droplets in the cytoplasm. Bar, 5 μm. (D) and (E) Group 3: Thyroxine plus gonadotropin-treated *rdw* rats. Activated capillaries in developing CLs. (D) An endothelial cell (E) shows luminal cytoplasmic processes (arrowheads). A fibrocyte (F) adheres to the capillary with its long cytoplasmic processes (arrows). Note the presence of a capillary bud (asterisk). Bar, 5 μm. (E) Group 3: Thyroxine plus gonadotropin-treated *rdw* rats. A sprouting capillary in the CL. Two endothelial cells (1 and 2) show thin projections in the lumen (arrows). One of these endothelial cells (nucleus not included in the section) leads the sprout formation and the secondary lumen (arrowhead) organization. The other one is located at the beginning of the sprout. A tight junctions (white arrow) connects two endothelial cells. Note the presence of two pericytes (P) that closely envelope endothelial cells. F, fibrocyte; lc, luteal cells. Bar, 5 μm.

was hardly recognizable. Degenerative processes involved both granulosa and thecal cells. Capillary vessels were seen in the thin (15–25 μm) theca *interna*. They showed a round shape with a regular profile. Arterioles and venules were recognized in the thecal layer (Fig. 1B). Transmission electron microscopy showed thecal capillaries, characterized by a regularly shaped round or oval lumen in cross-section (Fig. 2B). As in control rats, endothelial cells were flat and provided with a smooth plasma membrane, and oval regular nuclei with substantial heterochromatin (Fig. 2B). Differently, rare pericytes with short cytoplasmic extensions were observed around some capillaries (Fig. 2C). Thecal cells with signs of luteinization (mainly represented by an increased number of lipid droplets and cytoplasmic-nuclear ratio) were found after hCG administration (Fig. 2B, C). Scanning electron microscopy of gonadotropin-treated *rdw* rat ovaries did not present microvascular casts of CLs.

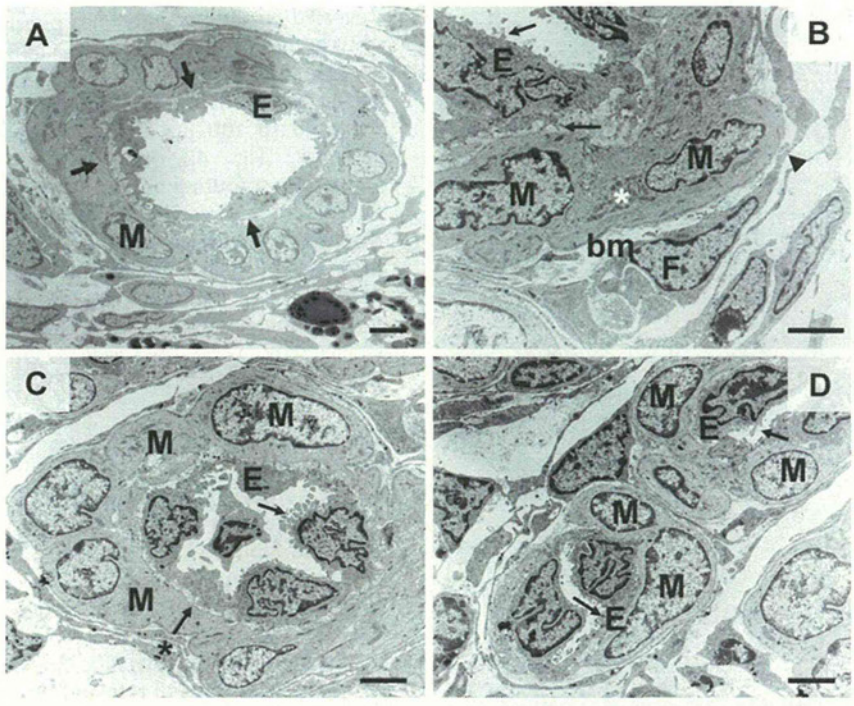

Fig. 3. Representative image of arterioles and venules, showing signs of angiogenic activation, in rat developing CLs. (A) Group 1: gonadotropin-treated Wistar-Imamichi rats (control): an arteriole. Round and swollen smooth muscle cells (M), whose nuclei are rich in heterochromatin, are separated from the adjacent luminal endothelial cells (E) by a subendothelial lamina (arrows). Note the irregular and abundant luminal cytoplasmic protrusions of endothelial cells. Bar, 5 μm. (B) Group 1: gonadotropin-treated Wistar-Imamichi rats (control): a venule. The wall of the venule, partially sectioned, shows numerous luminal and abluminal villous-like processes (arrows) of the endothelial cells (E). The smooth muscle cell (M) cytoplasm is abundant and rich in organelles (asterisk). A fibrocyte-like cell (F), with a regular nucleus, envelops with its protrusions (arrowheads) the smooth muscle cells outside the basement membrane (bm). Bar, 5 μm. (C) Group 3: thyroxine plus gonadotropin-treated *rdw* rats: an arteriole. Numerous cytoplasmic processes are present in the luminal surface of the endothelial plasma membrane (arrow). The endothelial cell nuclei show an irregular profile. The endothelial cell (E) lay down on a subendothelial lamina (asterisk plus arrow). Note the general hypertrophic aspect of the microvessels (in particular those of smooth muscle cells, M). F, fibrocytes. Bar, 5 μm. (D) Group 3: thyroxine plus gonadotropin-treated *rdw* rats: two venules. Cytoplasmic processes (arrows) protrude to the lumen of the venules. Endothelial cell (E) nuclei, polyhedral in shape and with an irregular profile, occupy a large amount of the cytoplasm. Smooth muscle cells (M) appear swollen and disposed in a single layer. Bar, 5 μm.

3.1.3. Group 3: T4 plus gonadotropin-treated rdw rats

Light microscopy of group 3 ovaries showed several developing CLs (Fig. 1C) together with healthy and atretic antral FLs. A thin capsule of connective tissue, in which arterioles and venules were recognized, encircled the CLs. Luteal cells, organized in clusters of few elements (between three and 10 cells), were immersed in a fine net of connective tissue containing numerous capillaries, similar to that observed in group 1. CL cell cytoplasm contained many lipid droplets (Fig. 1C). By TEM, luteal capillaries showed frank morphologic signs of activation such as flat or pocket-like lumen sometimes with a sinusoidal profile, thick heteromorphic endothelial cells with irregularly shaped nuclei, and numerous processes in both luminal and stromal sides of their plasma membrane (Fig. 2D, E). Endothelial cells adhered to each other through intact tight junctions (Fig. 2E). Different to group 2, most capillaries appeared activated as demonstrated by irregular luminal and abluminal cytoplasmic protrusions of different thickness and size, increase in the chromatin density, irregular basement membrane, sprouting, and budding. Several pericytes were always observed in proximity of activated capillaries (Fig. 2E, Table 1). Often, in correspondence of endothelial sprout origin, pericytes embraced and accompanied sprout formation with several cytoplasmic processes (Fig. 2E). Pericyte nuclei were round and rarely lobulated (Fig. 2E). Sometimes, stromal fibrocyte-like cells (e.g., quiescent fibroblasts characterized by a large nucleus, thin, flattened cytoplasm, and not actively secreting collagen fibers) were seen close to activated capillaries. These cells were distinguished by pericytes for their position, outside of the vascular basal membrane and were provided with long cytoplasmic processes that surrounded capillaries (Fig. 2D, E).

In CL, numerous small arterioles and postcapillary venules were seen (Fig. 3C, D). These vessels showed polyhedral, thick endothelial cells, provided with irregularly shaped nuclei and very numerous microvillous-like processes. A dense subendothelial lamina was present. Perivascular smooth muscle cells, generally monolayered, were voluminous, provided with an oval central nucleus, and normally distributed cytoplasmic organelles (Fig. 3C, D). By SEM of vcc, the surface of each ovary of group 3 showed four to five spherical small luteal VPs (diameter 1.2–1.4 cm) (Fig. 4B, C). Straight small terminal arterioles (diameter, 30–40 μm) supplied the luteal VPs. A dense and intricate capillary network, originating from these arterioles, penetrated and partially filled the luteal VP, as

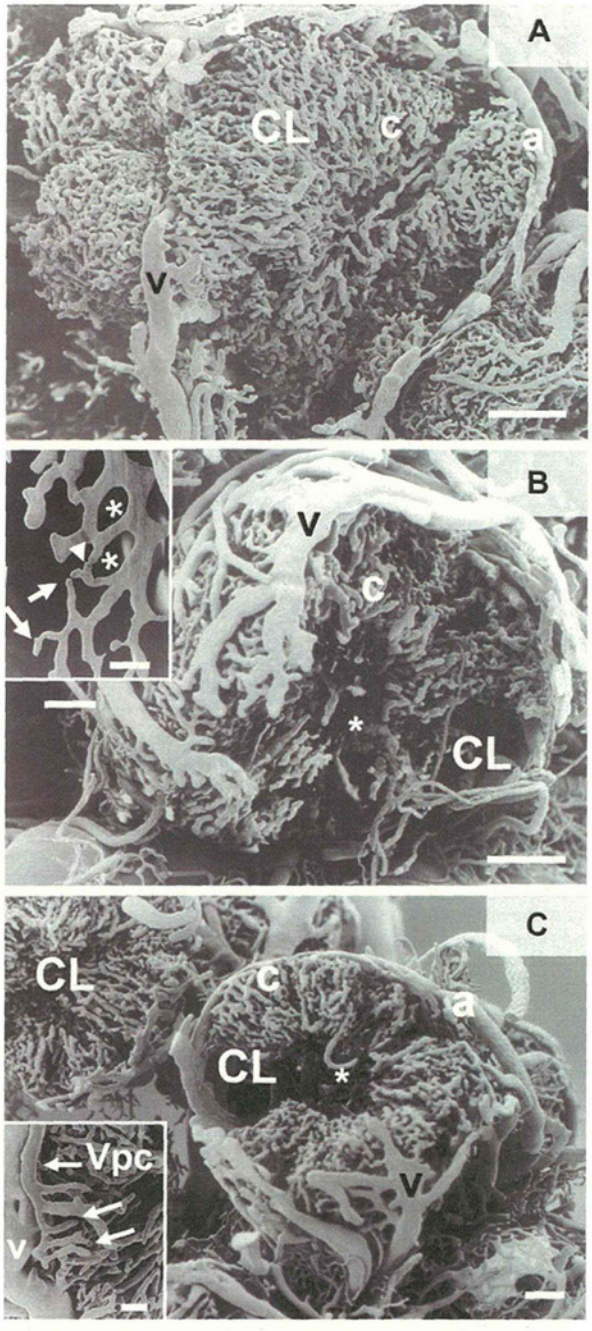

Fig. 4. Representative images of the outer surface of rat developing CLs by scanning electron microscopy of vascular corrosion casts. (A) Group 1: gonadotropin-treated Wistar-Imamichi rats (control). The dense vascular network of the CL is characterized by small caliber capillaries (c) growing toward the avascular central cavity. The developing CL is supplied by a system of arterioles (a) and drained by venules (v). Bar, 200 μm. (B) and (C) Group 3: thyroxine plus gonadotropin-treated *rdw* rats. Three luteal vascular plexuses in the ovarian cortex. An abundant superficial system of drainage, made of flattened venules (v), covers the great part of the plexuses. Note the presence of small arterioles (a) supplying the CLs. A copious network of capillaries (c) originates from these arterioles. Note also the presence of a poorly vascularized area in the center of CLs (asterisks). (B) Bar, 200 μm. (C) Bar, 100 μm. (B, inset) A portion of the luteal capillary network is seen at higher magnification: note the organization in large meshes (*). Numerous angiogenic figures, i.e., characteristic blood vessel formations indicating angiogenesis, such as sprouts (arrows) and vesicular buds (arrowheads) are present. Bar, 50 μm. (C, inset) A portion of the drainage system of a luteal vascular plexus in the ovarian cortex. The luteal capillaries are drained by small postcapillary venules (Vpc), which are collected by a wide system of large and flattened venules of drainage (v). From the Vpc often originated capillaries of neoformation in the form of blind endings of the resin (venular angiogenesis) (arrows). Note the tortuous course of the luteal capillary vessels. Arrows indicate sprouts. Bar, 50 μm.

revealed by the presence of a poorly vascularized area in the center of these plexuses (Fig. 4B, C). At higher magnification, tortuous and dilated capillaries (diameter 12–13 μm), arranged in irregular polygonal large meshes (ranging from 50 to 100 μm in size) formed a luteal capillary network (Fig. 4B, inset). These capillaries showed numerous sprouting angiogenic figures such as buds and sprouts of the resin (Fig. 4B, inset). CL capillaries were drained by small postcapillary venules (diameter 20–40 μm) (Fig. 4C, inset). These venules often originated capillaries of neoformation in the form of blind endings of the resin (venular angiogenesis). Postcapillary venules were collected by a wide superficial system of large and flattened venules of drainage (diameter 80–120 μm) (Fig. 4C, inset).

3.2. Quantitative study of pericytes

The number (mean ± SD) of follicular and luteal capillaries did not vary among the three experimental groups ($P > 0.05$; Table 1). The number of pericytes (mean ± SD) in CL capillaries of T4 plus gonadotropin-treated *rdw* rats (group 3) was similar to that found in control CLs. CL capillaries were not present in group 2 (Table 1). Pericytes in follicular capillaries significantly decreased in group 2, compared with control rats and group 3 ($P < 0.001$). The total number of pericytes was significantly higher in groups 1 and 3 than in group 2 ($P < 0.001$; Table 1).

3.3. Molecular study

Thyroxine treatment significantly increased mRNA expression levels of VEGF and bFGF in group 3 ovaries (containing many CLs), when compared with those of group 2 (where no CL was found in the ovaries), and showed values comparable with those obtained in group 1 (Fig. 5). More specifically, VEGF mRNA expression, when compared with group 1 (relative ratio ± SD, 10.167 ± 0.764), significantly decreased in group 2 (8.333 ± 0.289; $P < 0.05$) and increased in group 3 (9.5 ± 0.5; $P < 0.05$). Similarly, bFGF mRNA expression significantly decreased in group 2 (5.333 ± 0.557) compared with group 1 (7.633 ± 0.551; $P < 0.01$). Thyroxine (group 3) restored an expression pattern of bFGF similar to those found in group 1 (7.967 ± 1.05; $P > 0.05$; group 2 vs. group 3: $P < 0.05$). No differences were detected in the other growth factors analyzed (TGFβ-1, EGF, TNFα) ($P > 0.05$) (Fig. 5A, B).

4. Discussion

Thyroxine supports fertility restoration in immature infertile spontaneous hypothyroid *rdw* rats by inducing, in combination with gonadotropins, functional changes

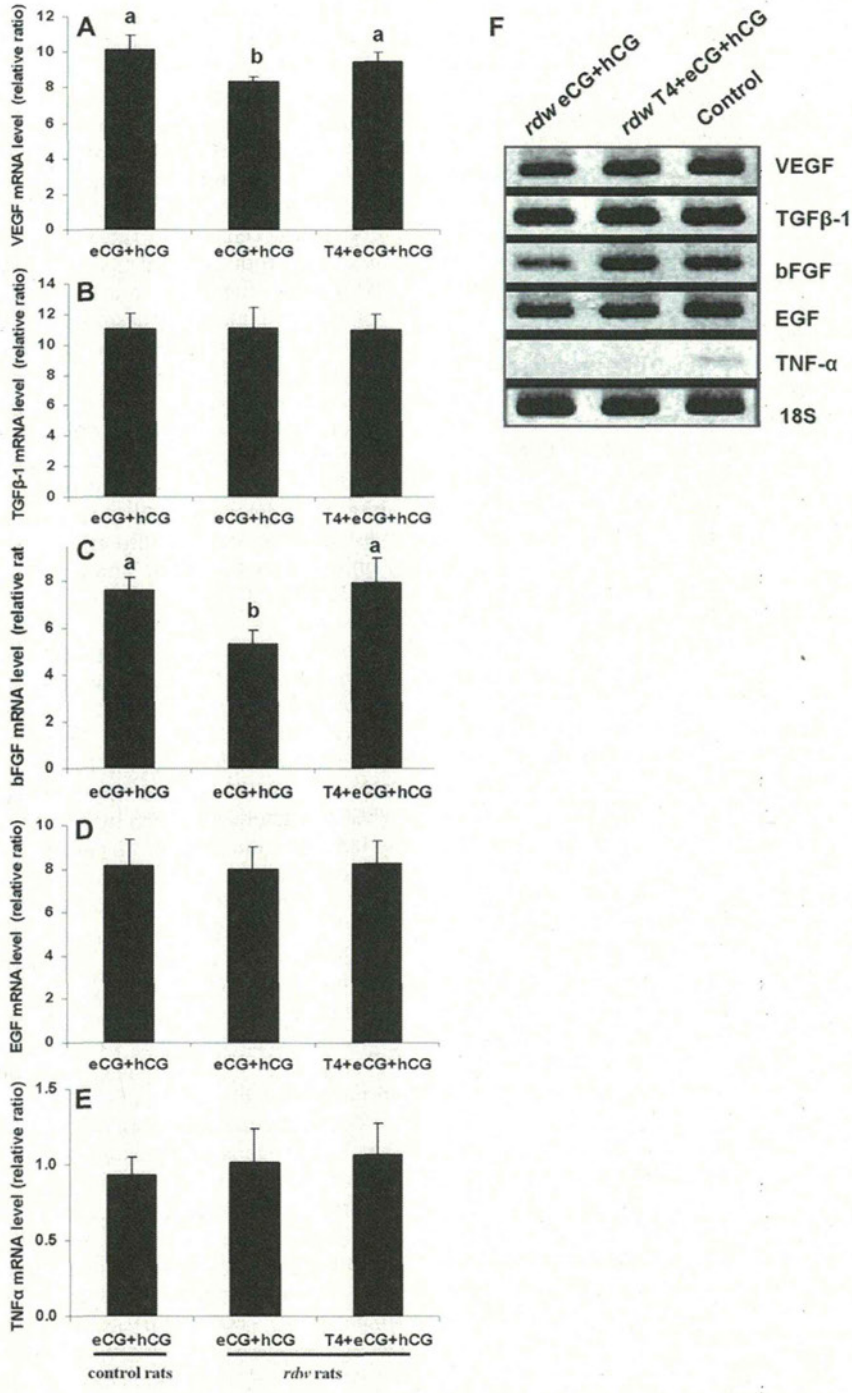

Fig. 5. mRNA expression pattern of growth factors involved in the regulation of angiogenesis. (A) Expression of mRNA for vascular endothelial growth factor (VEGF) (A), transforming growth factor (TGF)β-1 (B), basic fibroblast growth factor (bFGF) (C), epidermal growth factor (EGF) (D), tumor necrosis factor (TNF)-α (E) by reverse transcriptase polymerase chain reaction (RT-PCR) in ovaries of: group 1, control rats; group 2, gonadotropin-treated *rdw* rats; group 3, thyroxine plus gonadotropin-treated *rdw* rats. Results are representative of three separate experiments on whole ovaries obtained from two animals per each experimental group. Data are represented as mean ± SD of the relative ratio between each angiogenic factors and 18S RNA. Significant differences are represented by small letters ($P < 0.05$). (F) A representative image of RT-PCR is shown.

such as increased follicular development, augmented plasma estradiol levels [25], and improved percentage of fertilized eggs producing live pups [24,38]. It also promotes angiogenesis in ovarian FLs of *rdw* rats by upregulating mRNA expression of major angiogenic factors [19].

Because angiogenesis has a key role in the correct accomplishment of the ovarian function [1–5,8–10,19,

32,39,40], we aimed to study the effects of T4 and gonadotropin administration on postovulatory microcirculation and angiogenesis in female *rdw* rats. The results obtained showed for the first time that T4, in combination with eCG and hCG, modulated CL angiogenesis by the upregulation of angiogenic growth factors expression, such as VEGF and bFGF, associated with endothelial cell and pericyte activation and proliferation.

Gonadotropins are the primary factors with angiogenic potentiality—involved in FL development and CL formation [17]—interacting with thyroid hormones. Experimental studies performed *in vivo* and *in vitro* demonstrated that T4 is able to act as a "biological amplifier" of the action exerted by FSH in the functional differentiation of granulosa cells at several levels. In particular, T4 cooperates with hypophysary gonadotropins in promoting granulosa cell morphological differentiation, LH receptor acquisition, and steroidogenic enzyme (3β-hydroxysteroid dehydrogenase and aromatase) synthesis [21,41–43]. However, the fact that not only granulosa cells but also stromal cells, cumulus cells, and oocytes of different mammals express thyroid hormone receptors [41–44], suggests a wider action field of thyroid hormones in the ovary, involving factors such as integrins and growth factor receptors. Thyroxine preferentially binds αVβ3 integrins to stimulate mitogen-activated protein kinase (MAPK)-dependent angiogenesis [45,46]. Integrin αvβ3, the vitronectin receptor, is expressed by vascular cells and is upregulated during sprouting angiogenesis [47]. It has been shown that αVβ3 integrin interacts with growth factor receptors such as VEGF receptor 2, fibroblast growth factor (FGF) receptor 3, epidermal growth factor receptor and platelet-derived growth factor receptor [48], all triggering the angiogenesis signaling cascade. Thyroxine, indeed, exerts the proangiogenic action that we observed in this study by activating αVβ3 integrins, which cross-talk with adjacent VEGF and bFGF receptors [29]. Moreover, T4 could probably also exert an action on pericyte recruitment and activation by interacting with the platelet derived growth factor receptor of pericytes, whose mRNA expression increased after hCG-induced ovulation [49].

In this study, the evidence of a combined angiogenic action of T4 and gonadotropins was proved by the growth of developing CLs provided with an extensive capillary network only in the T4 plus gonadotropin group, as occurred in control rats. Morphologic data showed several activated capillaries with angiogenic figures (budding and sprouting) in the CL parenchyma, and they were associated with numerous pericytes enveloped in a basal membrane that is continuous with the endothelial basal membrane [50]. The endothelium of growing luteal capillaries evidenced typical angiogenic ultrastructural parameters, such as highly variable shape, increment of plasma membrane specializations, and presence of irregularly shaped nuclei. Moreover, budding and sprouting of capillaries from preexisting vessels are considered to be proliferative (angiogenic) features [4,5,33,34]. The microvascular activation after T4 supplement was so intense that it involved the entire microvascular compartment of the CL, as shown by the presence of numerous arterioles and venules with voluminous and swollen smooth muscle cells. The growth of these bigger vessels serves to supply an adequate blood flow necessary to sustain the increased metabolic needs of the growing CL [9,10].

In presence of T4 (group 3) the total number of follicular and luteal pericytes (determined considering that the CL capillaries are formed from the invasion of thecal capillaries into the avascular antral cavity of the FL as a consequence of the angiogenic process [36]) around the activated endothelial cells of *rdw* rats were significantly higher than in gonadotropin-treated *rdw* rats (group 2) and comparable with those found in control rats, as confirmed by the quantitative analysis. These results further evidenced that T4 exerts a proangiogenic action by activating the recruitment of pericytes, essential in the first hours after ovulation [14,15,51,52]. Pericytes act by modulating the migration of thecal endothelial cells in the postovulatory FL wall, to organize the neoformation and maturation of luteal capillaries [3,14,53]. The activity of pericytes is particularly intense in developing CLs where they secrete intercellular vesicles, then convert into empty "spikes" releasing their content (growth factor and/or cytokine) after reaching target cells [16].

Numerous experimental results demonstrated that crucial events such as folliculogenesis, follicular atresia, luteogenesis, and luteolysis are locally regulated by angiogenic factors produced by different ovarian cell populations (thecal cells, granulosa cells, luteal cells). Ovarian angiogenic factors mainly belong to VEGF and FGF families of proteins [13,52,54–59]. During the early luteal stages [54], VEGF is actively expressed by luteal granulosa cells in both nonprimate and primate CL [13,53–55]. Vascular endothelial growth factor, which is induced both by the hypoxic environment in the ovulated FL and by hCG [56], plays a well established role as stimulator of endothelial cell proliferation and activator of antiapoptotic pathways [57]. Another key regulator of luteal angiogenesis is FGF [58] and, analogously to VEGF, its production in luteinizing granulosa cells increases in the early stages of luteal development [52], specifically during endothelial cell sprouting and tubule initiation [59].

The molecular data obtained by RT-PCR demonstrated that T4 plus gonadotropins allow the expression of luteal angiogenic factors in *rdw* rats and restore an expression pattern overlapping that of gonadotropin-primed animals (control rats). In particular, the T4 plus gonadotropin administration significantly increased mRNA expression levels of the two main growth factors regulating luteal angiogenesis, VEGF and bFGF. The lack of development of CLs in *rdw* rats treated only with gonadotropins is a direct consequence of the reduced expression of VEGF and bFGF, as shown in cow [60], where the CL growth was significantly impaired after neutralization of VEGF and bFGF. Remarkably, the increased expression of VEGF and bFGF mRNAs observed in T4 plus gonadotropin-treated *rdw* rats is in agreement with data obtained in cow developing CL [15], where the endothelial cells formed tubules under the influence of VEGFA and FGF2.

Compared with data previously obtained in ovarian FLs treated with T4 [19], relative ratios for the examined angiogenic factors increased in developing CL except for TNFα. These results are in agreement with data present in